Assessing the accuracy of the heat flux measurement for the study of boiling phenomena

M. Kim[a], A. Sergis[b], S. J. Kim[a*], Y. Hardalupas[b]

[a] Department of Mechanical Engineering, Korea Advanced Institute of Science and Technology, 291 Daehak-ro, Daejeon 34141, Republic of Korea

[b] The Department of Mechanical Engineering, Imperial College London, London SW7 2AZ, UK

[*]Corresponding author: Telephone: +82 (42) 350-3043, Fax: +82 (42) 350-8207, Email: sungjinkim@kaist.ac.kr

Abstract

The present work quantifies numerically the systematic errors present in experimental infrared heat flux studies of boiling surfaces. A transient conduction model for multilayer structures is proposed to describe the periodic heat fluxes encountered on boiling surfaces. The results of the current work show that the systematic error behavior of the infrared method is not uniform but dependent on the frequency of the heat flux signal of the boiling surface; which is a novel finding. As the frequency of the heat flux signal increases, the errors in the measured phase of heat flux signals are expected to increase. The errors in the amplitude of heat flux signals sharply increase at low frequencies (1-10 Hz) and decrease as the frequency increases. The maximum errors in the phase and amplitude of heat flux signals are 9% and 23%, respectively in the frequency range of nucleate boiling (10-80 Hz). Based on the current analysis, it is concluded that the systematic errors found arise from assuming that thermal contact resistances of such systems are negligible. This is an assumption universally adopted

by the field. By considering and correcting for the thermal contact resistance in the measurement of heat fluxes, the maximum errors in the phase and the amplitude of heat flux signals can be reduced to 7% and 9%, respectively. The results are applied to experimental data ensembles from the published public domain. Finally, the current work provides general guidelines to improve systematic errors in the measurement of heat flux for the study of boiling using infrared thermography found in the literature.

Keywords: Heat flux measurement, Infrared thermography, Nucleate boiling, Multilayer structure

Nomenclature

a	Coefficient of the discretization equation [J/(m^{2}K)]
b	Source term in the discretization equation [J/m^2]
c_p	Specific heat capacity [J/kg-K]
E	Radiation energy [W/m^2]
$F_{\lambda_1\text{-}\lambda_2}$	Fraction of the radiation between two wavelengths λ_1 and λ_2
f	Frequency [s^{-1}]
h	Heat transfer coefficient [W/(m^2-K)]
k	Thermal conductivity [W/(m-K)]
L	Thickness [m]
N	Grid number [-]
q''	Heat flux [W/m^2]
$\dot{q}$	Volumetric heat generation [W/m^3]
R	Reflectivity [-]
T	Temperature [K]
t	Time [s]

Greek symbols

α	Absorption coefficient [m^{-1}]
α_s	Thermal diffusivity [m^2/s]
δ	Thermal penetration depth [m]
ε	Emissivity [-]
θ	Thermal contact resistance [m^{2}K/W]
λ	Wavelength [m]
ρ	Density [kg/m^3]
σ	Stefan-Boltzmann constant [W/m^2·K^4]
τ	Transmissivity [-]
τ_c	Time constant [s]
ϕ	Phase angle [rad]
ω	Angle velocity [rad/s]

Subscripts

a	Arbitrary
b	Bottom
c	Camera
inf	Infinity
N	North
non	Non-dimensional
opaq	Opaque to infrared radiation
P	Present
p	Polyimide
S	South

si	Silicon
t	Top

1. Introduction

As heat flux from engineering devices increases, the need for effective thermal solutions is also increasing continuously. Boiling is a powerful solution for the cooling of high heat flux devices due to its high thermal performance. However, it is difficult to predict the accurate thermal performance of boiling because of its complex mechanism. Many investigators have tried to investigate the mechanism of boiling through the experimental observations. For example, Voglar *et al.* [1] measured the temperature distribution at the boiling surface using a high-speed infrared camera and Kim *et al.* [2] measured the liquid-vapor phase distribution using a high-speed infrared thermography technique called DEPIcT. Other researchers such as Gerardi *et al.* [3] and Surtaev *et al.* [4] measured the frequency and the diameter of vapor bubbles using the synchronized high-speed infrared and video cameras. Recently, several researchers [5-8] succeeded in measuring the heat flux distribution at the boiling surface. They used infrared (IR) thermography to measure the temperature distribution, and then solved the transient heat equation by using the measured temperature distribution as the boundary condition. Heat flux is calculated from the temperature gradient along the thickness direction of the heater used for boiling. Because the heat flux distribution provides crucial clues to the mechanism of boiling, measuring the accurate heat flux distribution is important for the study of boiling.

Jung and Kim [6] mentioned that the small uncertainty of temperature measurement may lead to errors in the heat flux measurement. This is because the uncertainty is amplified as the thickness of the heater used for boiling decreases. In periodic heating, the phase and the amplitude of temperature signals depend on thermal mass and thermal resistances of the system [9]. As such, if inaccurate values of thermal mass and thermal resistances for the heating system are used, errors in the phase and the amplitude of heat flux signals are caused. Previous researchers [5-8] assumed that the thermal contact resistances of the system and the thermal

masses of IR-opaque layers are negligible when solving the heat equation to process their recorded data. These assumptions may lead to significant errors in the phase and the amplitude of heat flux signals. An assessment of the accuracy of these assumptions has not been published. Possible systematic errors induced by such assumptions need to be investigated quantitatively.

In the present study, systematic errors in the heat flux measurement for the study of boiling are numerically quantified. A transient conduction model for multilayer structures is proposed to describe the periodic heat flux condition on the heater used for boiling. The numerical code for the proposed model is validated by reproducing the experimental results of lock-in thermography. Systematic errors in the phase and the amplitude of heat flux signals are evaluated in the frequency range of boiling (1-80 Hz). The results are in good agreement with the experimental results of Jung *et al.* [7]. A parametric study is conducted to identify the effect of thermal mass and thermal contact resistances to heat flux signals. The current authors are working on an experimental method to model the heat flux signals encountered on boiling surfaces and hence fully and quantitively evaluate the suggested systematic errors from the current numerical work in high temporal and spatial accuracy.

2. Methodology

2.1. Heat flux measurement for the study of boiling

Jung *et al.* [7] are popular researchers in the field of IR heat flux measurements for the study of boiling. They measured temporal and spatial temperature distributions at fluid-wall interfaces through specially designed infrared (IR) transparent heaters. They subsequently used the data to calculate heat flux distributions at fluid-wall interfaces during pool boiling. Their measurement method is based on the IR thermography technique developed by Kim *et al.* [10]. The key feature of the technique is the use of IR transparent materials to form the heater which is proposed by Gerardi *et al.* [3]. In the study of Jung *et al.* [7], silicon has been used as the heating element sandwiched with a polyimide layer acting as an electrical insulator followed by an IR opaque layer to enable the acquisition of heat flux information at the fluid-wall interface. Additional layers may be further added on IR opaque layer to serve certain functions (i.e. waterproofing).

To obtain high-resolution temporal and spatial heat flux distributions at the fluid-wall interface, temperature profiles within the multilayer heater are required. These are unknown initially, but are obtained by solving the heat equation. Figure 1 shows the schematic diagram of the heating system that Jung *et al.* [7] used. The relation between the radiation energy signal and the temperature signal recognized by the IR camera is described in Eq. 2.1.

$$F_{\lambda_1-\lambda_2}\sigma T_{\mathrm{c}}^4(x,t) = E_{\mathrm{c}} = R_{\mathrm{inf-c}}E_{\mathrm{inf}} + \varepsilon_{\mathrm{si\text{-}c}}E_{\mathrm{si}} + \varepsilon_{\mathrm{p\text{-}c}}E_{\mathrm{p}} + \tau_{\mathrm{opaq\text{-}c}}E_{\mathrm{opaq}} \tag{2.1}$$

In here, $E_{\mathrm{inf}} = F_{\lambda_1\text{-}\lambda_2}\sigma T_{\mathrm{inf}}^4$ is the blackbody radiation due to surroundings, while $E_{\mathrm{si}} = \int_0^{L_{\mathrm{si}}} \alpha_{\mathrm{si}} F_{\lambda_1\text{-}\lambda_2}\sigma[T(x,t)]^4 e^{-\alpha_{\mathrm{si}}x}\mathrm{d}x$ is the total radiation energy emitted from the silicon layer that reaches the silicon-ambient interface. $E_{\mathrm{p}} = \int_0^{L_{\mathrm{p}}} \alpha_{\mathrm{p}} F_{\lambda_1\text{-}\lambda_2}\sigma[T(x,t)]^4 e^{-\alpha_{\mathrm{p}}x}\mathrm{d}x$ is the total radiation energy emitted from the polyimide layer that reaches the silicon-polyimide interface,

and $E_{\text{opaq}}=F_{\lambda_1\text{-}\lambda_2}\sigma[T(0,t)]^4$ is the blackbody radiation from the IR-opaque surface. Coefficients, $R_{\text{inf-c}}$, $\varepsilon_{\text{si-c}}$, $\varepsilon_{\text{p-c}}$ and $\tau_{\text{opaq-c}}$ are optical properties which are defined in the study of Kim *et al.* [10]. $F_{\lambda_1\text{-}\lambda_2}$ is the fraction of the total emission from a blackbody that is in a certain wavelength interval or band. It is defined as follows [9].

$$F_{\lambda_1-\lambda_2}=\frac{\int_{\lambda_1}^{\lambda_2}E(\lambda,T)d\lambda}{\int_0^{\inf}E(\lambda,T)d\lambda} \tag{2.2}$$

The temperature profile in the heater, $T(x,t)$ is obtained by solving the heat equation described in Eq. 2.3. The boundary condition is described in Eq. 2.4. T_{b} refers to the temperature value of the bottom surface of the heater used for boiling.

$$\rho_{\text{p}}c_{p,\text{p}}\frac{\partial T(x,t)}{\partial t}=k_{\text{p}}\left(\frac{\partial^2 T}{\partial x^2}\right) \quad \text{at} \quad 0\le x<L_{\text{p}}$$

$$\rho_{\text{si}}c_{p,\text{si}}\frac{\partial T(x,t)}{\partial t}=k_{\text{si}}\left(\frac{\partial^2 T}{\partial x^2}\right)+\dot{q}''' \quad \text{at} \quad L_{\text{p}}\le x<L_{\text{p}}+L_{\text{si}} \tag{2.3}$$

$$T\left(L_{\text{p}}+L_{\text{si}},t\right)=T_{\text{b}}(t) \tag{2.4}$$

As shown in Eq. 2.3 and Eq. 2.4, an additional boundary condition is required to solve the heat equation. The radiation energy balance equation, described in Eq. 2.1, was used for the additional condition in solving the heat equation. By coupling these equations, the temperature profile, $T(x,t)$ is obtained. Heat flux at the interface between the IR opaque layer and the polyimide layer is calculated from Eq. 2.5.

$$q''_{\text{opaq-p}}=k_{\text{p}}\left.\frac{\partial T(x,t)}{\partial x}\right|_{x=0} \tag{2.5}$$

Throughout this process, Jung *et al.* [7] made two assumptions:

a. Heat flux at the fluid-wall interface is same as heat flux at the interface between the IR-opaque layer and the polyimide layer.
b. Thermal contact resistances at each interface are negligible.

These assumptions are widely used and accepted in the heat flux measurement for the study of boiling. The validity of these assumptions is investigated in this paper to verify their accuracy. More specifically, the assumptions are tested numerically to ensure the lack of systematic errors arising by the possible presence of phase lag and amplitude discrepancies between the calculated heat flux signal and the real one at the fluid-wall interface. The presence of non-linear systematic phase lag between heat flux signals will result in incoherency in the temporal evolution of events imaged between the fluid-wall interface and the wall-polyimide interface. Any occurrence of amplitude shifts between heat flux signals at the fluid-wall interface and the wall-polyimide interface will lead to wrong estimations of heat flux. As such, it is crucial to resolve, understand and analyze the possibility of these errors in order to improve the accuracy of the heat flux measurement employed in the field.

To check the validity of these assumptions, the heat transfer model is developed in the next section. The heat equation and the corresponding boundary conditions for the multilayer structure are proposed to describe the periodic heating encountered on boiling surfaces. By solving the equation, the systematic error caused by the assumptions can be estimated.

2.2. Formulation of the heat transfer model

Generally, the thickness of the heater used for boiling is much thinner than the width of the heater. As such, a homogeneous and infinitely large plate with a multilayer structure is considered to model the system (See Fig. 2). The plate consists of thermally different layers, labelled 1 to n. The different layers are separated by planar interfaces (at $x=x_i$ with $i=1, \cdots, n\text{-}1$). The thermal properties of the assembled system consist of the thermal

conductivity k_i, density ρ_i, and specific heat $c_{p,i}$ with i=1, 2, ⋯, n for each layer. The heat source is applied to layer 1 in the form of joule heating, where Layer 1 is the top layer of the system. The location and form of the heat source are selected in order to imitate the periodic heat transfer phenomena on Surface 1 (at x=x_1) in boiling. The volumetric heat generation rate in Layer 1 is assumed to be $\dot{q}_1(1+0.5\sin(\omega t))$ where $\dot{q}_1$ is the average volumetric heat generation rate in Layer 1 and ω is the angular speed of the heat source. In each layer, the temperature distribution follows the classical thermodynamic relation:

$$\rho_1 c_{p,1}\frac{\partial T}{\partial t} = k_1\frac{\partial^2 T}{\partial x^2} + \dot{q}_1\left(1+0.5\sin(\omega t)\right) \quad \text{at} \quad 0 < x < x_1 \tag{2.6}$$

$$\rho_i c_{p,i}\frac{\partial T}{\partial t} = k_i\frac{\partial^2 T}{\partial x^2} \quad \text{at} \quad x_i < x < x_{i+1}, \quad i = 1,2,\cdots \tag{2.7}$$

The heat transfer boundary conditions are as follows.

(i) At the top surface (x=0)

$$-k_1\left.\frac{\partial T}{\partial x}\right|_{x=0} = h_t\left(T_{\inf} - T\big|_{x=0}\right) \quad , \quad t > 0 \tag{2.8}$$

(ii) At the interfaces between two layers (x=x_i with i=1, 2, ⋯, n-1)

$$k_i\left.\frac{\partial T}{\partial x}\right|_{x=x_i^-} = k_{i+1}\left.\frac{\partial T}{\partial x}\right|_{x=x_i^+} \tag{2.9}$$

$$\frac{T\big|_{x=x_i^+} - T\big|_{x=x_i^-}}{\theta_{i,i+1}} = k_{i+1}\left.\frac{\partial T}{\partial x}\right|_{x=x_i^+} \quad \text{with} \quad i = 1,\ 2,\ \cdots,\ n-1,\ \ t > 0 \tag{2.10}$$

(iii) At the bottom surface (x=x_n)

$$-k_n\left.\frac{\partial T}{\partial x}\right|_{x=x_n} = h_b\left(T\big|_{x=x_n} - T_{\inf}\right), \quad t > 0 \tag{2.11}$$

where h_t is the convective heat transfer coefficient at the top surface, h_b is the convective heat transfer coefficient at the bottom surface, T_{inf} is ambient temperature, and $\theta_{i,i+1}$ is the thermal contact resistance on Surface i which is the interface between Layer i and Layer i+1.

2.3. Numerical approach

To solve the heat equation described in Section 2.2, the system was discretized as shown in Fig. 3. There were N grid points and the grid size was fixed to Δx. The time difference between successive time steps was Δt. The solution was obtained by marching in time from a given initial temperature distribution. The initial temperature distribution was given as $T(x, 0) = T_{inf}$. The discretization equation was derived by integrating Eqs. 2.6 and 2.7 over the control volume in Fig. 3 and over the time interval from t to $t + \Delta t$. The fully implicit scheme was used. The derived discretization equation is described as follows:

$$a_P T_i^{t+\Delta t} = a_S T_{i-1}^{t+\Delta t} + a_N T_{i+1}^{t+\Delta t} + b \tag{2.12}$$

where

$$a_P = \rho_i c_{p,i} \Delta x - 2k_i \frac{\Delta t}{\Delta x},\ a_N = k_i \frac{\Delta t}{\Delta x},\ a_S = k_i \frac{\Delta t}{\Delta x},\ b = \rho_i c_{p,i} \Delta x T_P^t .$$

At the surface between the adjacent layers, the coefficients of Eq. 2.12 are as follows.

(i) Top surface

$$a_P = \rho_1 c_{p,1} \frac{\Delta x}{2} + k_1 \frac{\Delta t}{\Delta x} + h_t \Delta t,\ a_N = k_1 \frac{\Delta t}{\Delta x},\ a_S = 0,\ b = h_t T_{inf} \Delta t + \rho_1 c_{p,1} \frac{\Delta x}{2} T_1^t + \frac{\dot{\ }}{2} \Delta x \left(1 + 0.5 \sin(\omega t)\right)$$

(ii) Contact region between Layer i and Layer i+1

$$a_P = \frac{\Delta t}{\theta_{i,i+1}} + \frac{\Delta t}{\theta_{i,i+1}},\ a_N = \frac{\Delta t}{\theta_{i,i+1}},\ a_S = \frac{\Delta t}{\theta_{i,i+1}},\ b=0$$

(iii) Bottom surface

$$a_P = \rho_N c_{p,N} \frac{\Delta x}{2} + k_N \frac{\Delta t}{\Delta x} + h_b \Delta t,\ a_N = 0,\ a_S = k_{N-1} \frac{\Delta t}{\Delta x},\ b = h_b T_{inf} \Delta t + \rho_N c_{p,N} \frac{\Delta x}{2} T_P^t$$

The Tridiagonal Matrix Algorithm method (TDMA) [11] was applied to solve the above discretization equations. Compared to the explicit forward difference method, the implicit scheme is stable for any size of the time step. Also, the TDMA method has a benefit of reducing the calculation time compared to the Jacobi or Gauss-Seidel iterative method. For these reasons, the fully implicit scheme and the TDMA method were used to solve the heat equation.

2.4. Phase lag calculations

Phase lag is the angular cycle equivalent of the time lag between the measured heat flux signal and the actual one on the boiling surface. The temporal response analysis of the system is investigated to examine possible effects of multilayer thermal mass interactions that might affect the accuracy of the heat flux measurement described in Section 2.1. This exercise is of particular importance upon progressing the present work towards a fully bound experiment in the future and, as such, these experimentation challenges are also taken into account at this stage. In the heat transfer model for multilayer structures described in Section 2.2, the heat flux signal at an arbitrary point (x=x_a , $0 < x_a < x_n$) is assumed to vary periodically with the same frequency of the heat source. Because of thermal inertia and heat diffusion phenomena, the temporal response of the heat flux signal is expected to be different compared to the excitation from the heat source at a given spatial point inside the system. As such, the phase angle of the heat flux signal at a certain distance from the heat source (ϕ_a) is different with that of the heat source signal. The absolute time lag is calculated by dividing the phase angle difference between these two signals by the angular velocity of signals.

$$\Delta t[s] = \frac{\phi_a}{\omega} = \frac{\phi_a}{2\pi f} \tag{2.13}$$

The non-dimensional time lag is obtained by multiplying the absolute time lag by the frequency of the signals (please note that the frequency signals remains the same).

$$\Delta t_{\text{non}}[-] = f \times t = \frac{\phi_{\text{a}}}{2\pi} \tag{2.14}$$

2.5. Model evaluation

The phase of the temperature signal is a complex function of the material's thermal properties, the modulation frequency of the signal and the configuration of the subsurface structure. The latter property is of particular importance in laminated systems where imperfections, especially in the deposition or/and adhesion of the layers, might become important. As such, if common defects like delamination occur near the material surface, the phase of temperature might change according to the ideal modelled case. Bai and Wong [12] analytically predicted and experimentally measured the phase difference between defective and non-defective areas of laminated structures (carbon-fiber-reinforced polymers, CFRPs) using lock-in thermography. The experimental method detects and compares the dynamic temperature response of a system between "healthy" and artificially defective areas as those are periodically thermally excited by IR light. Their work measured the phase lag characteristics of the temperature signal in the defective areas compared to the excitation signal. The research group also developed a method to analytically model the system, which was in good agreement with the experimental results. The minor differences between experiments and modeling were due to specimen manufacturing tolerances, which could not be included into the analytical 1D solution while the experimental results were affected by the 3D nature of the defects, adding uncertainties in the final prediction.

Bai and Wong [12] obtained an analytic solution by assuming that the solution of the heat equation is expressed as the sum of sine and cosine terms. According to this assumption, the boundary conditions are applied to the heat equation and the coefficients of the solution were obtained. The inverse matrix was used to solve the equation. The numerical solution in the current study obtained by the TDMA method and the fully implicit scheme is able to

simulate transient and steady state heat transfer in complex systems (via an iterative process spatially and temporally), while the model used by Bai and Wong [12] can only simulate the latter (no iterations in the temporal domain). As such, the heat transfer model developed in this study is more suitable for the analysis of boiling than the model used by Bai and Wong [12]. The model developed in the current study was used to reproduce the numerical and experimental results recorded by Bai and Wong [12] (Fig. 4). It is clear that the numerical predictions of the two models are almost identical, although the new method is different. Both numerical models present differences relative to the experiments because the effects of manufacturing tolerances in the specimen used by Bai and Wong [12] have not been considered in the current method. Nevertheless, the comparison provides a first evaluation of the newly developed analytical model of the current work before advancing to more complex cases.

2.6. Heater design for numerical simulation

The numerical model is employed to predict phase lags and amplitude discrepancies in the heat flux measurement. The heater design for numerical simulation is described in Fig. 5. The heater used for boiling consists of 5 layers (n=5 with thickness parameters: x_1=0.5 μm, x_2=1 μm, x_3=1.5 μm, x_4=11.5 μm and x_5=511.5 μm. The geometry of the heater is based on the design that Jung *et al.* [7] used in their work (Fig. 1). The black paint layer is replaced with the indium tin oxide layer. This is because the black paint can be easily damaged and detached from polyimide at high temperatures (about 160℃). The current improved geometry (without the Nichrome heater used to model boiling) is experimentally used in our group to study boiling effects. The silicon and polyimide layers in the current geometry are used for the same purpose as in the system of Jung *et al.* [7] i.e. as the primary heater and thermal insulation (to minimize heat flux bleating in directions perpendicular to the x-axis of the system as defined in the current manuscript). In order to simulate the transient heat transfer phenomena at the top layer, a nichrome layer and a silicon dioxide layer are added to the heater. The nichrome layer is used

for Layer 1 as a volumetric joule heater, and the silicon dioxide layer is used for Layer 2 as an electrical insulation. The reason of simulating the additional two layers instead of simply imposing a periodic heat flux boundary condition in the computational domain, is to allow conducting future experiments to validate the results in the current study taking into account the dynamic response a real boiling modelled system.

Surface 1 corresponds to the fluid-wall interface and hence measuring the heat flux signal on Surface 1 as accurately as possible is important to ensure the accuracy of the method. However, only the heat flux signal on Surface 3 can be measured using the infrared measurement technique introduced in Section 2.1. This is because the indium tin oxide layer is opaque to infrared radiation while the silicon and polyimide layers are not. Therefore, the accuracy of the measurement technique should be verified by comparing the heat flux signal on Surface 1 to the heat flux signal recorded on Surface 3.

The thermal properties of each layer are summarized in Table 1. The notion of an "effective thermal contact resistance" between each layer is introduced in this section. These are additional thermal resistances, which are primarily accounted from layer thermal contact resistances (due to surface bonding or material imperfections) and material manufacturing dimensional tolerances. There is no analytical method to calculate the effective thermal contact resistances for each layer as these are largely based on the manufacturing method used (which can be different from sample to sample and are expected to be of a 3D nature). As such, models with zero, moderate (based on experience and literature [13-14]) and high effective thermal contact resistances [15] are used for this analysis. The moderate effective thermal contact resistances at each interface are selected as $\theta_{1,2}$=10 cm^{2}K/W, $\theta_{2,3}$=10 cm^{2}K/W, $\theta_{3,4}$=0.1 cm^{2}K/W, $\theta_{4,5}$=0.1 cm^{2}K/W. These are chosen based on the reasoning that $\theta_{1,2}$ and $\theta_{2,3}$ must be larger than $\theta_{3,4}$ and $\theta_{4,5}$ because ceramic materials have poor bonding strength with metal and ceramic materials compared to polymers. The volumetric heat generation $\dot{q}_0$ is

selected as $20\ \mathrm{W/mm^3}$, which is similar to the expected heat flux value when the onset of nucleate boiling occurs during pool boiling of FC-72. The expected heat transfer coefficients at the top and bottom surfaces, h_t and h_b, are set to $9.4\ \mathrm{W/m^2{\cdot}K}$, $4.7\ \mathrm{W/m^2{\cdot}K}$. The heat transfer coefficients are selected by the correlations for natural convection that exist in the literature [16].

3. Results and discussion

3.1. Systematic errors of the heat flux measurement

To check the validity of the two assumptions in Section 2.1, the heat flux signal on the fluid-wall interface and the heat flux signal measured by the method of Jung *et al.* [7] should be compared to each other. As shown in Fig. 5, there are four surfaces in the heater. The heat flux signal on each Surface was obtained by solving the heat equation with the boundary conditions described in Fig. 5 and Table 2. The heat flux signal on Surface i is defined as $q_i(t)$ with i=1,2,3,4. In here, $q_1(t)$ corresponds to the heat flux signal on the fluid-wall interface and $q_3(t)$ corresponds to the heat flux signal on the interface between the IR opaque layer and the IR transparent layer. To obtain the heat flux signal measured by the method of Jung *et al.* [7], the temperature signal on Surface 3 ($T_{\mathrm{IR}}(x_3,t)$) was obtained by the method described in Section 2.1. Then, the heat equation was solved with the boundary conditions described in Fig. 6 and Table 2. Although there is the effective thermal contact resistance on Surface 4, it was neglected when the heat equation is solved. The heat flux signal on Surface 3 obtained by this method is defined as $q_{3,\mathrm{IR}}(t)$. The comparison between $q_1(t)$, $q_3(t)$ and $q_{3,\mathrm{IR}}(t)$ is illustrated in Fig. 7. Note that normalized heat flux is calculated by using Eq. 3.1.

$$\text{Normalized heat flux}\left[-\right] = \frac{q(t) - f\int_0^{1/f} q(t)\,dt}{\text{Amplitude}\left(q_1\right)} \tag{3.1}$$

A periodic heat source excitation signal (q_1, black line) is applied to Surface 1 of the system, which results in a periodic response of the heat flux signal with the same frequency on Surface 3 (q_3, red line). The blue line corresponds to $q_{3,\mathrm{IR}}$, which is the heat flux signal on Surface 3 measured by the method of Jung *et al.* [7]. To begin with, the assumption of approximating q_3 to q_1 appears to be inaccurate since it introduces non-linear systematic errors in the results for phase lag and the amplitude shift between heat flux signals on Surface

1 and Surface 3. Both errors of the phase and the amplitude increase as the frequency increases (with the exception of very low excitation frequencies where all signals are matched well). Moving on to the assumption of neglecting thermal contact resistances of the system, it is observed that $q_{3,\mathrm{IR}}$ is different with q_3. Even though the phase difference between $q_{3,\mathrm{IR}}$ and q_3 is negligible, the amplitude difference between $q_{3,\mathrm{IR}}$ and q_3 is significant. The amplitude difference between $q_{3,\mathrm{IR}}$ and q_3 increases at thermal excitation frequencies ranging from 1 Hz to 10 Hz but reduces towards higher frequencies. Overall significant deviations are found when $q_{3,\mathrm{IR}}$ is approximated q_1.

To quantify these deviations, non-dimensional time lag and the maximum relative error in the amplitude of heat flux are calculated and plotted against the frequency of the heat source excitation signal (Fig. 8 and Fig. 9). Non-dimensional time lag which is the ratio of time lag to the period of the excitation signal is calculated from Eq. 2.14, and the maximum relative error in the amplitude of the heat flux signal is calculated using Eq. 3.2.

$$\text{Maximum error of the amplitude}(\%) = \frac{\text{Amplitude}(q) - \text{Amplitude}(q_1)}{\text{Amplitude}(q_1)} \times 100\% \qquad (3.2)$$

As shown in Fig. 8, the non-dimensional time lag of q_3 and $q_{3,\mathrm{IR}}$ increases with the frequency. The time lag of $q_{3,\mathrm{IR}}$ has a similar trend as q_3 but values are different. The exact interaction physics of heat transfer in complex multi material systems (such as the one simulated) and the sensitivity of quantities, such as the time lag quantity and thermal signal amplitude, with varying material properties can only be revealed computationally. Nevertheless, general trends can be extracted and, up to a large degree, explained by classical physics. The thermal lag arises due to the process of energy transfer through the SiO_2 and indium tin oxide (ITO) layers. The thermal lag can be explained by the thermal time constant,

which is related to the heat transfer rate within the material. For a 3D material, this is described by:

$$\tau_c[s] = \frac{L^2}{\alpha_s} \tag{3.3}$$

The non-dimensional thermal time constant is defined classically by Eq. 3.4 [17], where α_s is the thermal diffusivity of material and L is the thickness of material. According to this definition, the non-dimensional thermal time constant can be calculated as follows, where f is the frequency of the external excitation heat source.

$$\text{non-dimensional time constant} = \tau_c \times f = \frac{L^2}{\alpha_s} f \tag{3.4}$$

As Equation 3.4 shows, for a given material, the non-dimensional time constant is expected to increase with increasing frequency, which is in agreement with general trend described in Fig. 8. However, material properties also affect this quantity. Additional 3D effective thermal contact resistances will be affecting the thermal diffusivity of material, which in turn will change the behaviour of the time lag. This is the reason why time lag of q_3 and $q_{3,\mathrm{IR}}$ are slightly different as shown in Fig. 8.

As shown in Fig. 9, q_3 shows a linear error in the amplitude of heat flux. The error is almost zero at low frequencies and gradually increases with frequency. The explanation of this behavior can be explained by the thermal penetration depth. The thermal penetration depth for a material is defined as the distance at which the temperature of the material has significantly changed with regards to the initial position of the application of thermal excitation as shown in Fig. 10. The thermal penetration depth is described as follows:

$$\delta = \sqrt{\frac{\pi \alpha_s}{f}} \tag{3.5}$$

where f is the frequency of the heat source excitation and α_s is the thermal diffusivity of the material. According to Eq. 3.5, the thermal penetration depth decreases with increasing frequency. Therefore, increasing the thermal excitation frequency on Surface 1 is expected to lead to reduction of the amplitude of the heat flux signal on Surface 3. This behavior is generally observed in Fig. 9 for q_3. Even though q_3 shows a linear relation with the frequency, $q_{3,IR}$ shows a non-linear behavior, which might be an indication of inaccurately modelled quantities. The error is sharply increased at low frequencies and gradually decreases from 10Hz onwards. The maximum error is 22% at 10 Hz which can be significant in the measurement of heat flux. As such, an investigation towards causes of the disparities detected between q_3 and $q_{3,IR}$ is needed to further understand the sources of error that might affect the accuracy of the method.

There are two differences between q_3 and $q_{3,IR}$. Firstly, $q_{3,IR}$ is calculated by the temperature boundary condition that is obtained by IR thermography. Secondly, the effective thermal contact resistance on Surface 4 is neglected when $q_{3,IR}$ is calculated (perfect system assumption). A deconstruction of the method is carried forward in order to determine which factor causes each of the observed error components. $q_{3,IR,th}$ is the approximated heat flux signal obtained by the method of Jung *et al.* [7] which is calculated again considering the "effective thermal contact resistance" on Surface 4. Information of boundary conditions used to obtain these signals (q, q_{IR}, and $q_{IR,th}$) are illustrated in Table 2. As shown in Fig. 8, there is still a negative phase lag at low frequencies. As such, it is deduced that the negative phase lag is due to the imposed temperature boundary condition, which is obtained from the IR thermography method. To obtain the temperature signal on Surface 3 by IR thermography, the coupled conduction and radiation equations have to be solved. Temperature is the effect of energy propagation; an approach, which utilizes a temperature boundary condition and works backwards to calculate the heat flux solution (causality), bypasses the history of the

temperature evolution, since thermal inertia effects from the entire system dictate this. This could be the reason why Jung's solution predicts an overall faster thermal response of the system even with the consideration of the effective thermal contact resistances. As shown in Fig. 9, the error in the amplitude of $q_{3,\mathrm{IR,th}}$ shows the same trend as the one of $q_{3,\mathrm{IR}}$. This means that the temperature boundary condition obtained by IR thermography might be the reason behind the non-linear relation with the frequency. The difference between the error in the amplitude of $q_{3,\mathrm{IR}}$ and that of $q_{3,\mathrm{IR,th}}$ can be explained by the thermal penetration depth described in Fig. 10. If the thermal contact resistance between the adjacent layers is neglected, the effective thermal conductivity of the system increases. According to Eq. 3.5, the thermal penetration depth increases as the thermal conductivity of the system increases. This results in an increase in the temperature amplitude at the interface between the IR opaque layer and the IR transparent layer as shown in Fig. 10. Because the amplitude of the temperature signal is proportional to the amplitude of the heat flux signal [9] in periodic heating, neglecting the thermal contact resistance causes the overestimation of the amplitude of the heat flux signal.

According to Gerardi *et al.* [18], the frequency range of nucleate boiling is from 10 Hz to 80 Hz for most cases. The nucleated bubble formation in pool boiling generally has a frequency range between 10 Hz and 80 Hz. As such, the maximum errors of about 8% for the non-dimensional time lag and 22% for the heat flux amplitude are expected according to the above results. While the maximum 8% error of non-dimensional time lag can be acceptable for the heat flux measurement, the maximum 22% error of the heat flux amplitude can be significant. The consideration of the thermal contact resistance ($\theta = 0.1$ cm^{2}K/W) can reduce the maximum error of the heat flux amplitude to 10%. Although the systematic error due to the imposed temperature boundary condition still remains, it compensates the error due to the assumption of approximating q_3 to q_1, especially at the high frequency range (40-80 Hz). As

such, just considering the thermal contact resistance seems to be enough to minimize the systematic error in the heat flux measurement using IR thermography.

Based on the results, it is concluded that the thermal mass of the infrared radiation (IR) opaque layer and the thermal contact resistance at the interface between the layers cause the systematic error in the measurement of heat flux using IR thermography. Therefore, those who want to measure heat flux using IR thermography are recommended to follow the guidelines presented below.

1. The number of layers that compose a heater should be minimized. The thermal contact resistance causes the error in the amplitude of the heat flux signal. Because the thermal contact resistance exists in every interface between the adjacent layers, the error in the amplitude of the heat flux signal can be reduced by minimizing the number of layers. It is practically recommended to use the heater that consists of only two layers. This is based on the fact at least two layers are required for the measurement of heat flux using IR thermography: one IR opaque layer and one IR transparent layer.
2. The thickness of the IR opaque layer should be minimized. The thermal mass of the IR opaque layer causes the time lag of the heat flux signal. Because the thermal mass is proportional to the thickness of the layer, the time lag of the heat flux signal can be reduced by minimizing the thickness of the IR opaque layer. Therefore, the thickness of the IR opaque layer should smaller than 2 μm. This is based on the fact the heat flux signal is significantly distorted if the time lag of the heat flux signal becomes larger than the time resolution of the IR camera which is about 1 ms. According to the numerical model in the current study, the time delay of the heat flux signal becomes larger than 1 ms when the thickness of the IR opaque layer becomes larger than 2 μm.
3. The accurate value of the thermal contact resistance should be used in estimating the heat flux using IR thermography. According to the current study, the systematic error can be

reduced by properly accounting for the thermal contact resistance in the estimation. Therefore, investigators have to find the value of the thermal contact resistance from literatures or experiments and use it when they solve the heat equation to obtain the heat flux signal.

3.2. Validation of the numerical results

To validate the numerical analysis method in the current study, the experimental results of Jung *et al.* [7] are used. Jung *et al.* [7] measured the temperature distribution at the boiling surface and converted it into the heat flux distribution using the method introduced in Section 2.1. Because Jung *et al.* [7] assumed that effective thermal contact resistances of the system were negligible, the heat flux distribution obtained by Jung *et al.* [7] might have systematic errors.

According to the results of the previous section, the experimental results of Jung *et al.* [7] can be improved by considering effective thermal contact resistances in measuring the heat flux distribution. Figure 11 shows the comparison between the modified and the original heat flux distribution. The modified heat flux distribution is obtained by considering the effective thermal contact resistance between the polyimide and the silicon layers ($\theta = 0.1$ cm^{2}K/W). The value of the effective thermal contact resistance is selected from the literature [13]. Figure 12 shows the comparison of the heat flux signals at the same point on each heat flux distribution in Fig. 11. The amplitude of the modified heat flux signal is smaller than the original heat flux signal, which is in good agreement with the results of Fig. 9.

To further model the amplitude difference between original and processed heat flux signals using the developed method, the broadband heat flux signals (as those found in boiling conditions - Fig. 12) are decomposed through the use of Fourier analysis (Fig. 13). It has been discovered that the dominant frequencies of the two heat flux signals are almost identical,

which means that the thermal contact resistance does not affect the frequency of the signal; as expected.

Figure 14 shows the first four most dominant heat flux signal frequencies present in the dataset of Jung *et al.* [7] as those are extracted from the analysis presented in Fig. 13. As shown in Fig. 14, frequency dependent non-uniform amplitude differences between the original and the modified signals exist. The relative error behavior of the amplitudes found from the results in Fig. 14 is expected to be similar in nature to that calculated from the results of Fig. 9. The result of this comparison is described in Fig. 15. As shown in Fig. 15, the trends of the two results are similar to each other which confirms the validity of the method used in the current work. The minor differences in the absolute values observed are due to the exact values of effective thermal contact resistances used in the analysis (in the current case, typical values are selected from the literature [13] that might differ slightly to the actual ones in the sample used).

3.3. Effects of the thermal contact resistance

The effects of selecting the thermal contact resistance and the systematic error sensitivity in the heat flux measurements are studied in the current section. The numerical simulations are performed by intentionally using higher effective thermal contact resistances expected for a substrate where a good bonding quality between the layers is not ensured [15]. This exercise highlights the resulting effects of manufacturing tolerances of similar systems for the use in the electronics industry. A case of zero effective thermal contact resistances (denoted by "θ, zero"), as per the assumption widely used in the field, and a case of high effective thermal contact resistances (denoted by "θ, high") are simulated. A case with average thermal contact resistances (found in the literature) is also contained for reference. The boundary conditions for the numerical simulation are listed in Table 3.

Figure 16 shows that significant errors are found in the calculation of time lag, particularly for higher thermal excitation frequencies. The zero effective thermal contact

resistance assumption creates a negative time lag (signal would appear to travel faster than what expected), while the high contact resistance assumption creates a positive time lag (signal would appear to travel slower than what expected) compared to the average thermal contact resistance case. The time lag seems to be highly sensitive to the choice of thermal contact resistances of the system. Thermal contact resistances are hard to measure experimentally and are believed to be controlled by the presence of manufacturing defects that are usually stochastic in nature. Caution is hence recommended when similar measurements are performed especially if different substrates are used for performing parametric studies for boiling.

The heat flux amplitude analysis for varying effective thermal contact resistances is presented in Fig. 17. The error is low for low thermal excitation frequencies, but significantly increases for high frequencies. The zero effective thermal contact resistance case leads to a gross overestimation of the heat flux amplitude on Surface 3, while the opposite happens for the case of high thermal contact resistances (deviations of more than 100% to the average thermal contact resistance case are observed). The error in the heat flux amplitude seems to be more sensitive to the choice of effective thermal contact resistances than the errors found for the temporal analysis of the system (time lags).

It is concluded that the choice of effective thermal contact resistance values to be used in the modelling of conduction in thin multilayer systems are crucial to the final accuracy of the results. It is also noteworthy to the readers that the results presented come from a 1D simulation. The 3D nature of a real system and the 3D non-uniform manufacturing tolerances to be encountered are expected to negatively and stochastically affect the predictions for real systems. Therefore, the present results underestimate the measurement errors of current advanced IR thermography methods. Care and caution are recommended for researchers in the field carrying out similar experimental investigations. A possible method to correct the experimental results is via the use of correction factors. This requires both a similar analysis as

the one presented in the current study and an additional experimental calibration process. This will form the topic of future work.

4. Conclusions

Numerical analysis was performed to quantify systematic errors in the heat flux IR thermography measurements for the study of boiling through transparent to IR radiation heaters. This type of experimental technique is widely employed by various researchers in the field. To describe the boiling heat transfer, a transient conduction model for multilayer structures was proposed. The numerical code for the proposed model was validated by reproducing experimental results obtained through lock-in thermography. It was discovered that systematic errors are present, non-uniform and depended on the frequency of the heat flux signals observed. As the frequency increases, errors in the phase of heat flux signals increase. On the other hand, errors in the amplitude of heat flux signals sharply increase at low frequencies (1-10 Hz) and then gradually decreased as the frequency is increased. The maximum errors in the phase and the amplitude of heat flux signals were 9% and 23%, respectively in the frequency range of nucleate boiling (10-80 Hz). Based on the numerical analysis, it was found that errors were mainly caused by the assumption that thermal contact resistances of the system were negligible. By considering the thermal contact resistance in the measurement of heat flux, the maximum errors in the phase and the amplitude can potentially be reduced to 7% and 9%, respectively. The improvement of systematic errors was validated by the use of experimental results from Jung *et al.* [7]. Researchers can estimate the systematic errors in the frequency range of interest using the presented technique. It is important to used the accurate value of thermal contact resistances in their measurement system to correct and minimize the systematic errors due to variabilities, imperfections, and manufacturing tolerances.

Acknowledgements

AS would like to thank the ERASMUS MUNDUS EASED program for awarding him a 6-month placement fellowship grant at KAIST (Grant 2012-5538/004-001) and CentraleSupélec as the coordinator of the grant. In particular, AS would like to thank Dr. Laurent Zimmer, Mrs. Lavinia Stanescu and Mrs. Aline Faes from the ERASMUS program for their gracious help facilitating the relocation at KAIST. Furthermore, AS would like to thank the EUROfusion committee, the host university KAIST and the home university Imperial College London that accommodated the ERASMUS placement during AS's running EUROfusion fellowship contract. Additional funding was supplied by the National Research Foundation of Korea (NRF) grant funded by the Korea government (MSIT) (No. 2012R1A3A2026427)

References

[1] J. Voglar, M. Zupančič, A. Peperko, P. Birbarah, N. Miljkovic, I. Golobič, Analysis of heater-wall temperature distributions during the saturated pool boiling of water, *Experimental Thermal and Fluid Science* 102 (2019) 205-214.

[2] D.E. Kim, J. Song, H. Kim, Simultaneous observation of dynamics and thermal evolution of irreversible dry spot at critical heat flux in pool boiling, *International Journal of Heat and Mass Transfer* 99 (2016) 409-424.

[3] C. Gerardi, J. Buongiorno, L. Hu, T. McKrell, Study of bubble growth in water pool boiling through synchronized, infrared thermometry and high-speed video, *International Journal of Heat and Mass Transfer* 53 (2010) 4185-4192.

[4] A. Surtaev, V. Serdyukov, J. Zhou, A. Pavlenko, V.Tumanov, An experimental study of vapor bubbles dynamics at water and ethanol pool boiling at low and high heat fluxes, *International Journal of Heat and Mass Transfer* 126 (2018) 297-311.

[5] I. Golobic, J. Petkovsek, D.B.R. Kenning, Bubble growth and horizontal coalescence in saturated pool boiling on a titanium foil, investigated by high-speed IR thermography, *International Journal of Heat and Mass Transfer* 55 (2012) 1385-1402.

[6] S. Jung, H. Kim, An experimental method to simultaneously measure the dynamics and heat transfer associated with a single bubble during nucleate boiling on a horizontal surface, *International Journal of Heat and Mass Transfer* 73 (2014) 365-375.

[7] J. Jung, S.J. Kim, J. Kim, Observations of the critical heat flux process during pool boiling of FC-72, *Journal of Heat Transfer* 136 (2014) 12 pages 041501

[8] V.S. Serdyukov, A.S. Surtaev, A.N. Pavlenko, A.N. Chernyavskiy, Study on local heat transfer in the vicinity of the contact line under vapor bubbles at pool boiling, *High Temperature* 56 (4) (2018) 546-552.

[9] F.P. Incropera, D.P. Dewitt, T.L. Bergman, A.S. Lavine, Principles of Heat and Mass Transfer 7th Edition, John Wiley & Sons, 2013, pp. 327-328, pp. 786.

[10]T.H. Kim, E. Kommer, S. Dessiatoun, J. Kim, Measurement of two-phase flow and heat transfer parameters using infrared thermometry, *International Journal of Multiphase Flow* 40 (2012) 56-67.

[11]S.V. Patankar, Numerical Heat Transfer and Fluid Flow, CRC Press, 2009, pp. 52-58.

[12]W. Bai, B.S. Wong, Evaluation of defects in composite plates under convective environments using lock-in thermography, *Measurement Science and Technology* 12 (2001) 142-150.

[13]A.M. Khounsary, D. Chojnowski, L. Assoufid, W.M. Worek, Thermal contact resistance across a copper-silicon interface, *High Heat flux and Synchrotron Radiation Beamlines* 3151 (1997) 45-51

[14]R.S. Prasher, J.C. Matayabas, Jr., Thermal contact resistance of cured gel polymeric thermal interface material, *IEEE Transactions on Components and Packaging Technologies* 27 (4) (2004) 702-708.

[15]D. Delaunay, P. Le Bot, Nature of contact between polymer and mold in injection molding. Part I: Influence of a non-perfect thermal contact, *Polymer Engineering and Science* 40 (7) (2000) 1682-1691.

[16]Y.A. Cengel, A.J. Ghajar, Heat and Mass Transfer Fundamental and Applications 4th Edition, McGraw-Hill, 2013, pp. 528.

[17]E. Marin, Characteristic dimensions for heat transfer, *Latin-American Journal of Physics Education* 4 (2010) 56-60.

[18]C. Gerardi (2009), Investigation of the pool boiling heat transfer enhancement of nano-engineered fluids by means of high-speed infrared thermography, Ph.D thesis, MIT, pp. 158.

List of figure captions

Fig. 17. Errors in the amplitude of heat flux signals (q_3, $q_{3,\theta,\,\mathrm{zero}}$, $q_{3,\theta,\,\mathrm{high}}$)

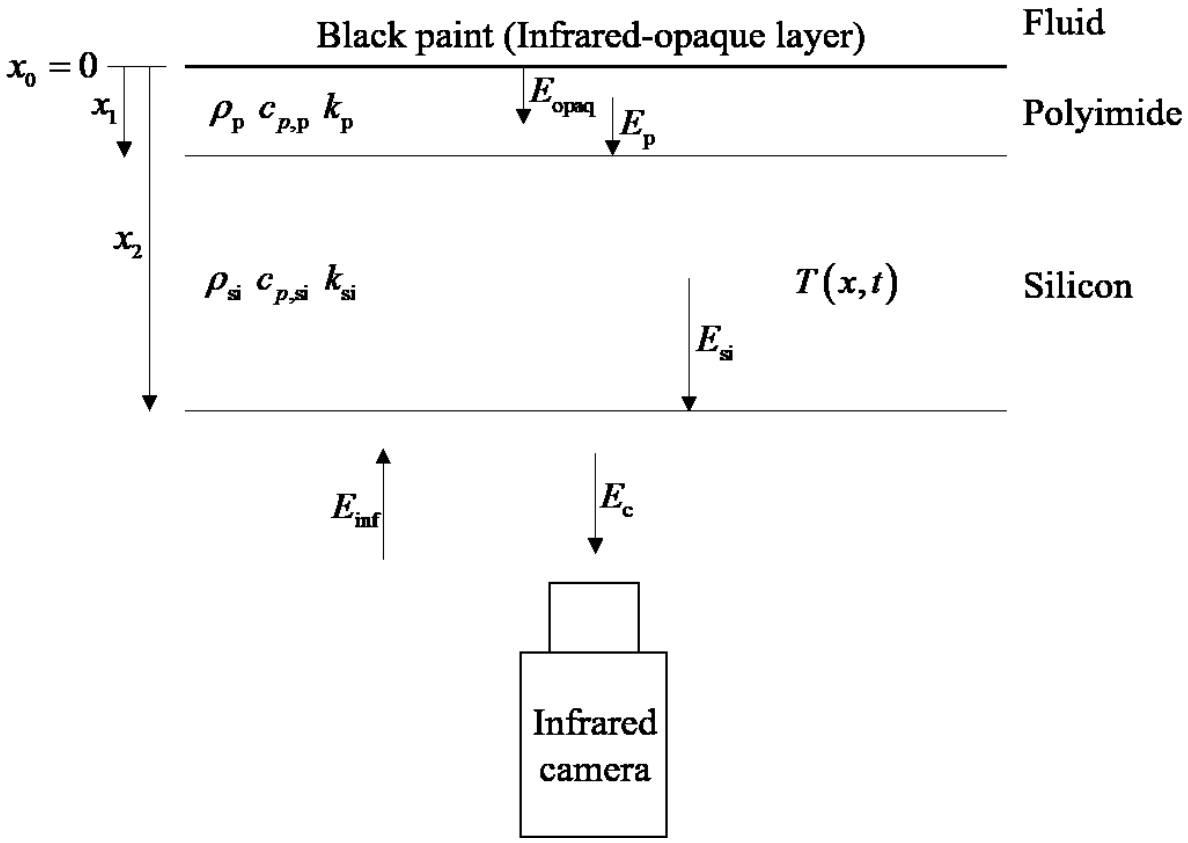

Fig. 1. Schematic diagram for infrared thermography

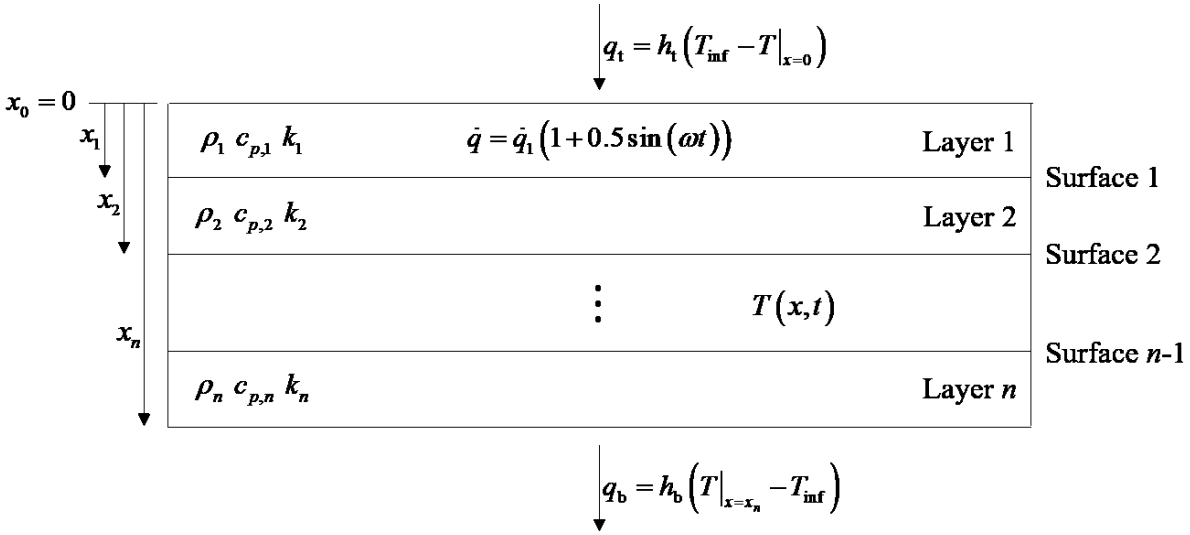

Fig. 2. Schematic diagram for the heat transfer model

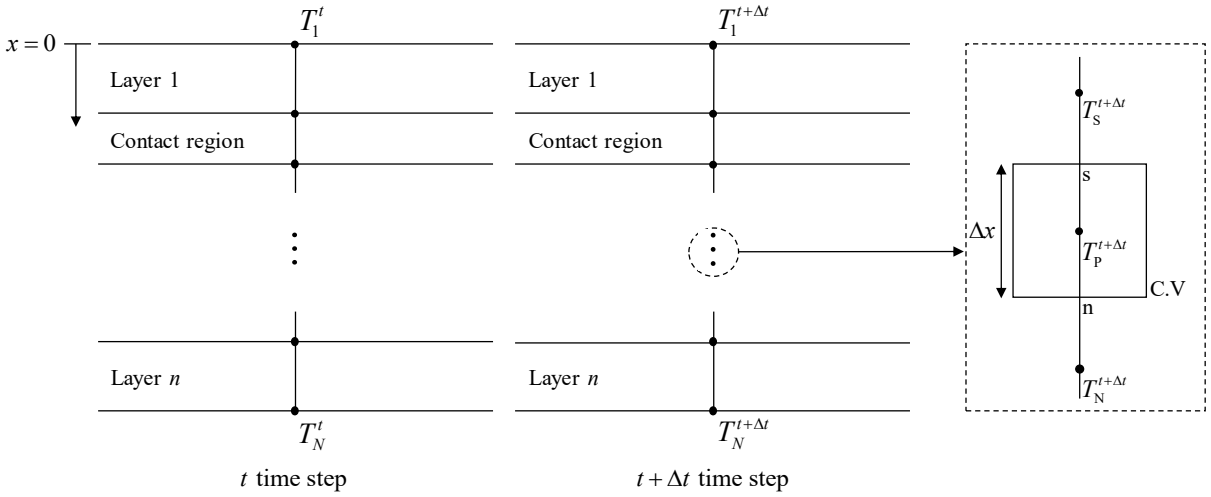

Fig. 3. Grid layout for numerical simulation

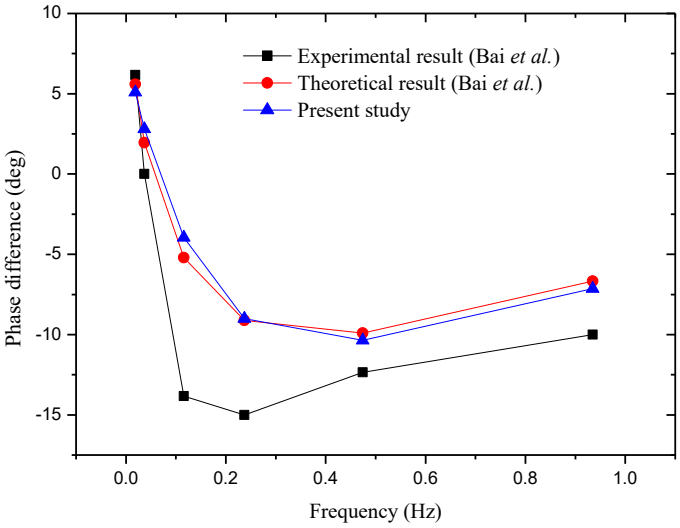

Fig. 4. Phase differences between defective areas and non-defective areas

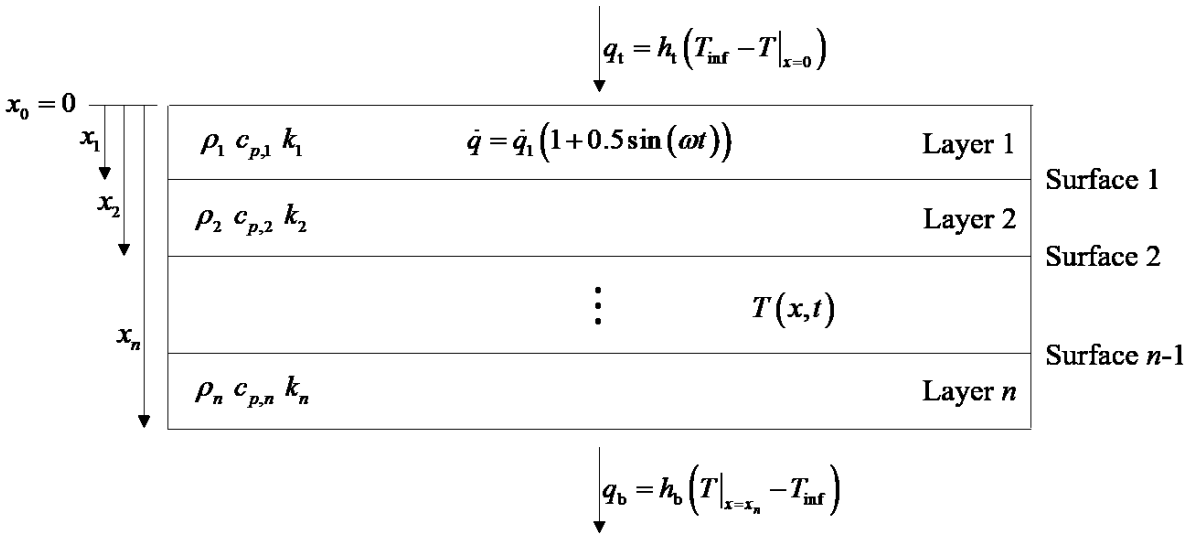

Fig. 5. Heater design used in the numerical simulations

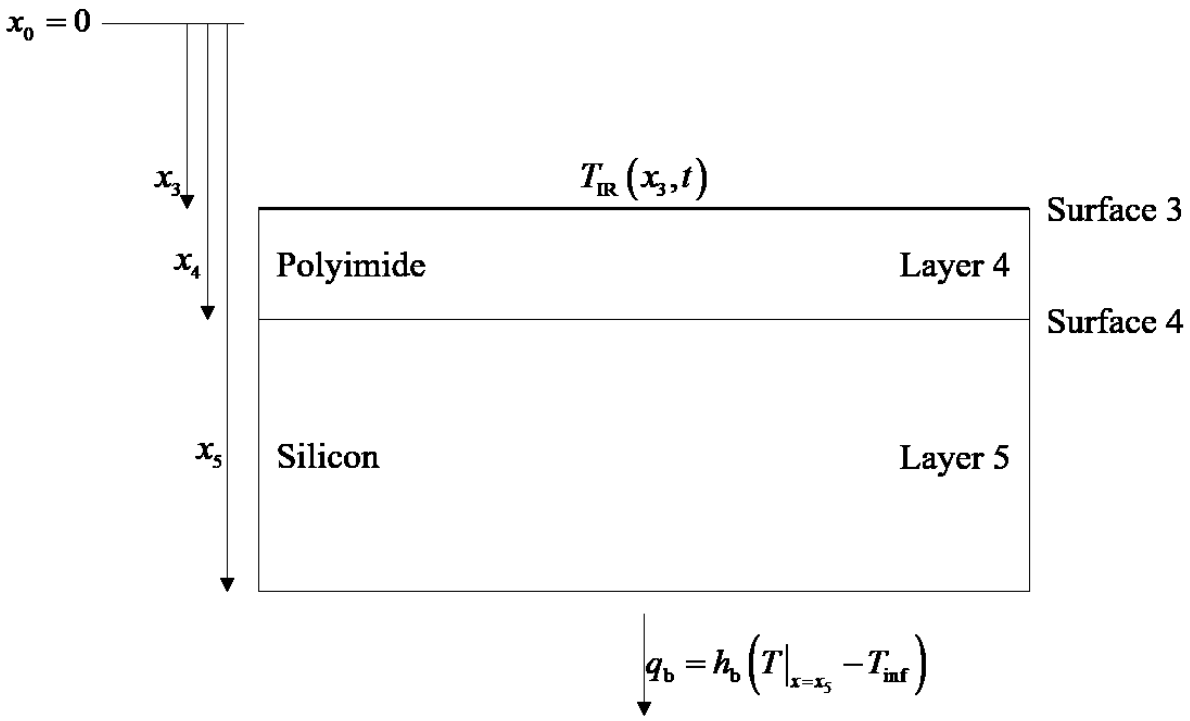

Fig. 6. Schematic diagram of boundary conditions used in the heat flux measurement

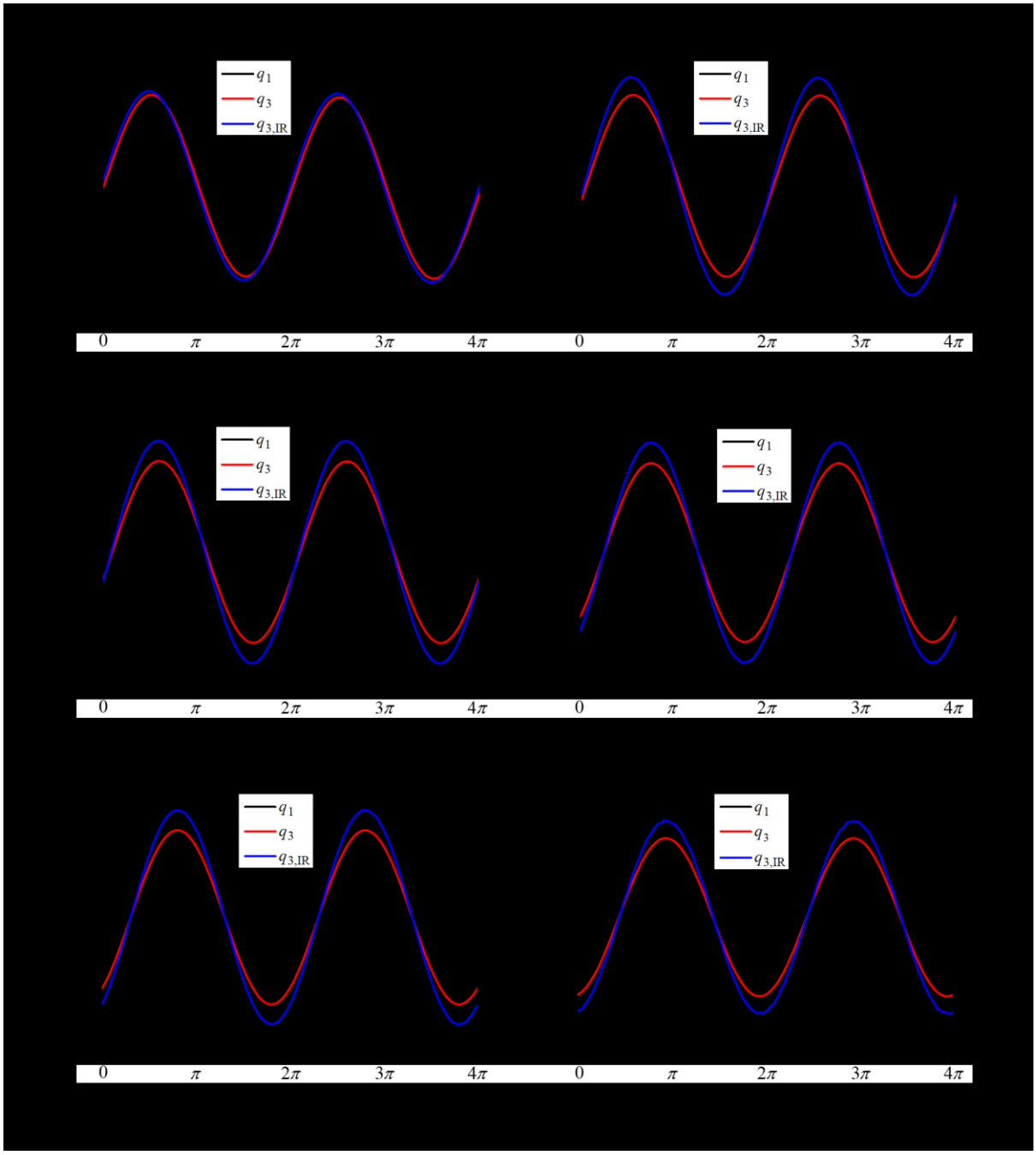

Fig. 7. Comparison of heat flux signals (q_1, q_3 and $q_{3,IR}$)

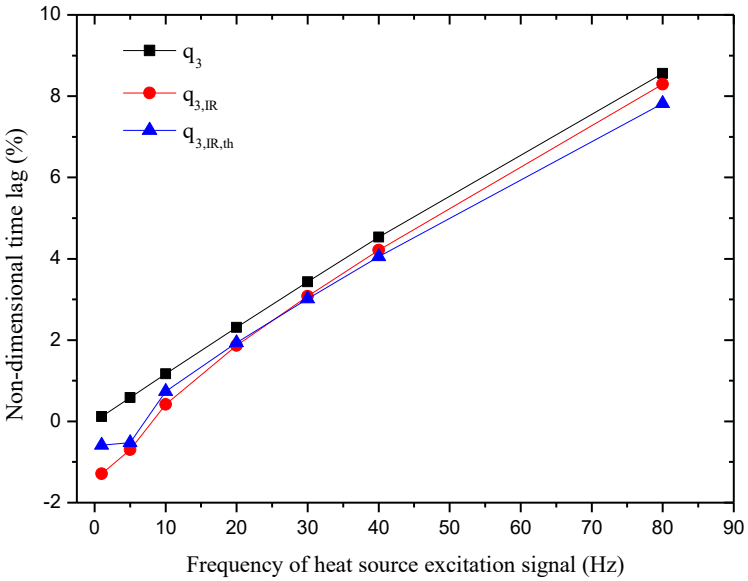

Fig. 8. Non-dimensional time lag of heat flux signals (q_3, $q_{3,IR}$, $q_{3,IR,th}$)

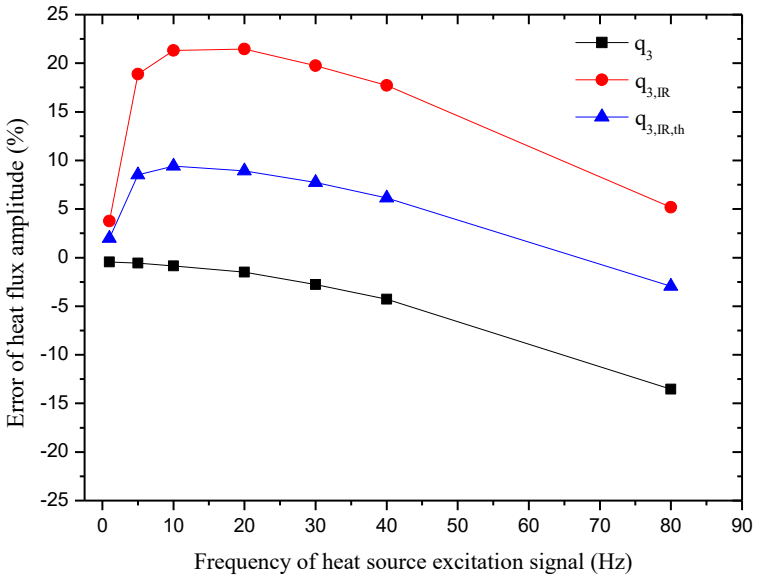

Fig. 9. Errors in the amplitude of heat flux signals (q_3, $q_{3,\mathrm{IR}}$ and $q_{3,\mathrm{IR,th}}$)

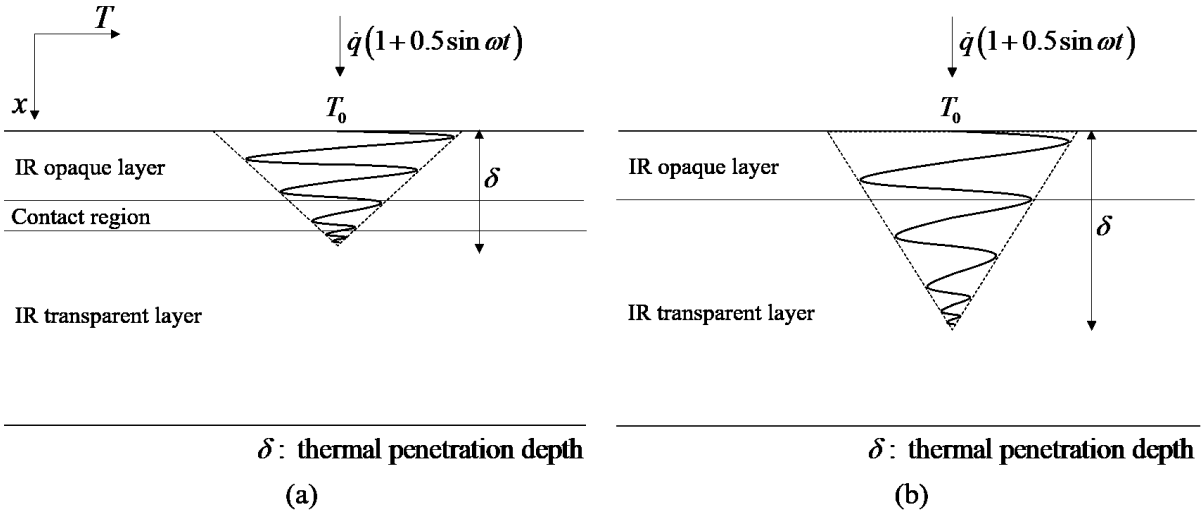

Fig. 10. Schematic diagram of the thermal penetration depth (a) when the contact region exists (b) when the contact region doesn't exist

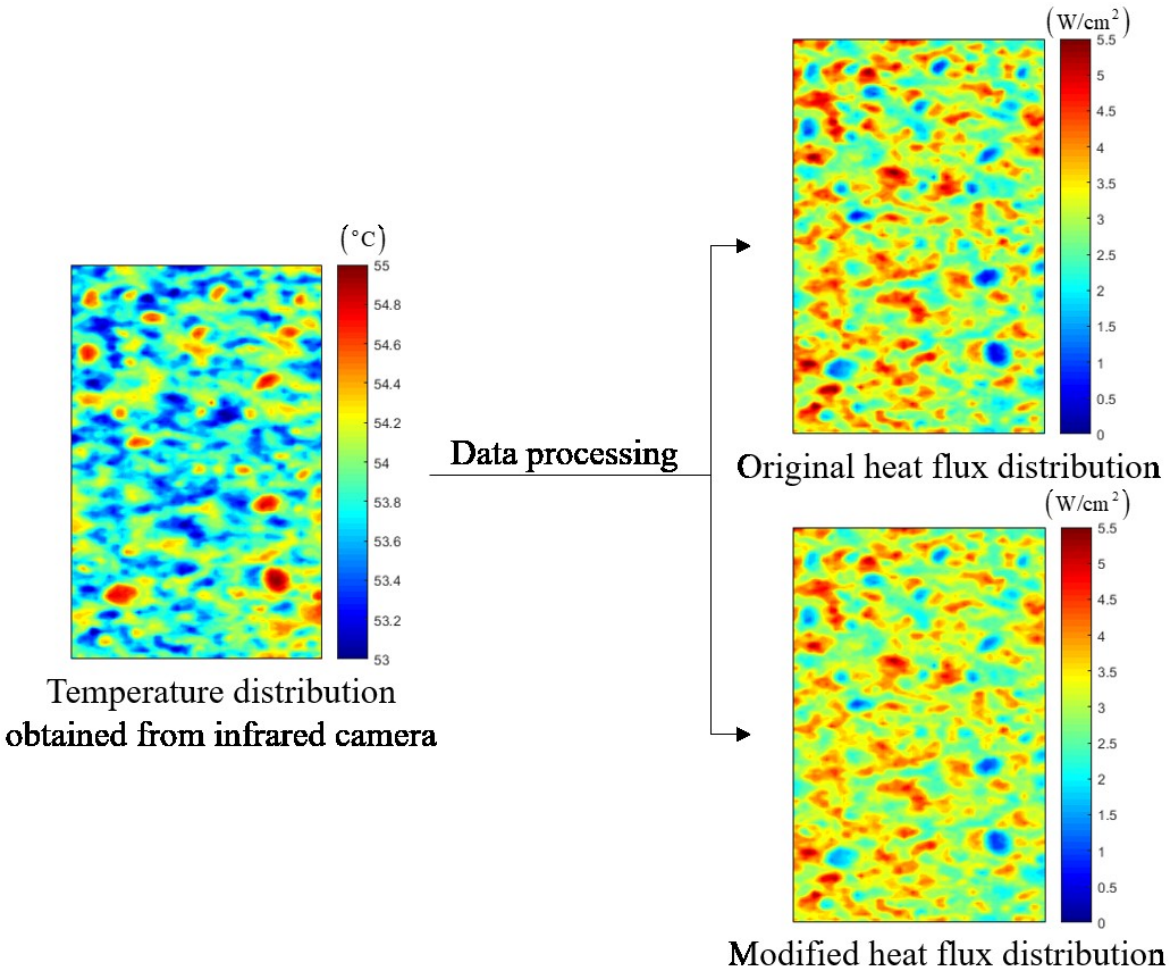

Fig. 11. Heat flux distributions obtained by Jung *et al.* [7]

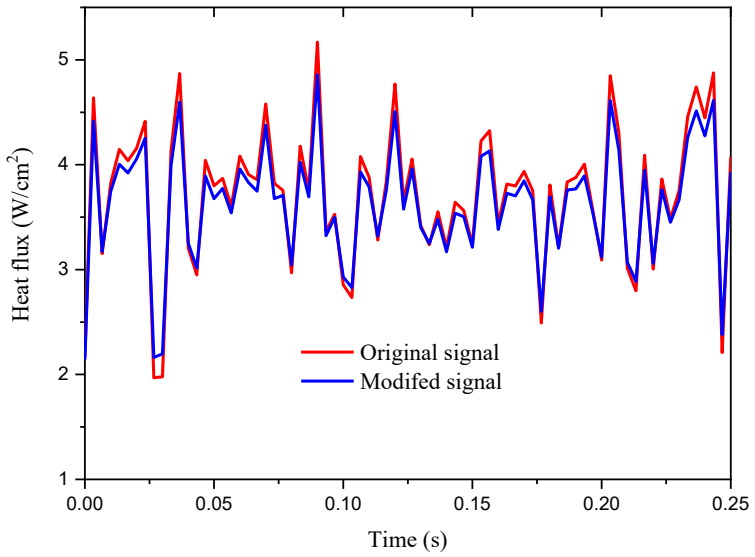

Fig. 12. Comparison between the original and modified heat flux signals

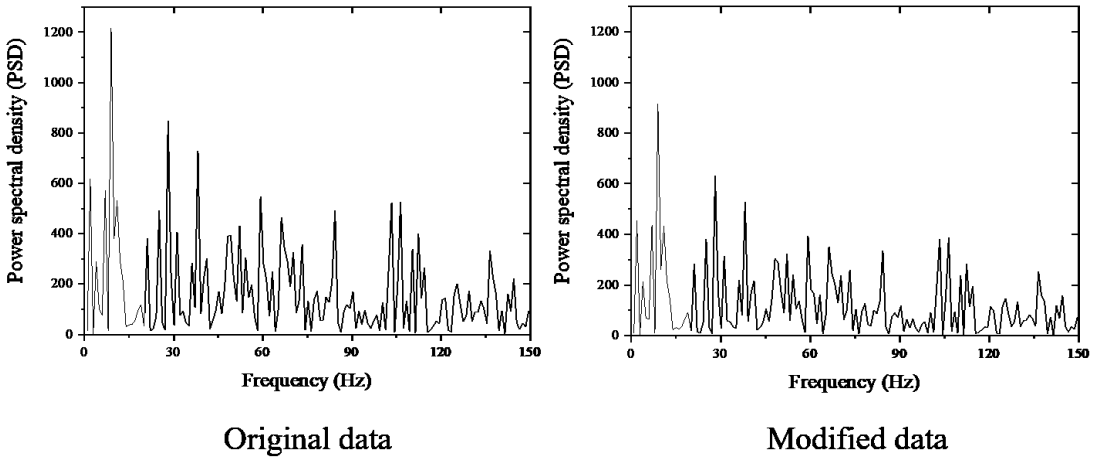

Fig. 13. Fourier analysis of (a) the original heat flux signal, and (b) the modified heat flux signal

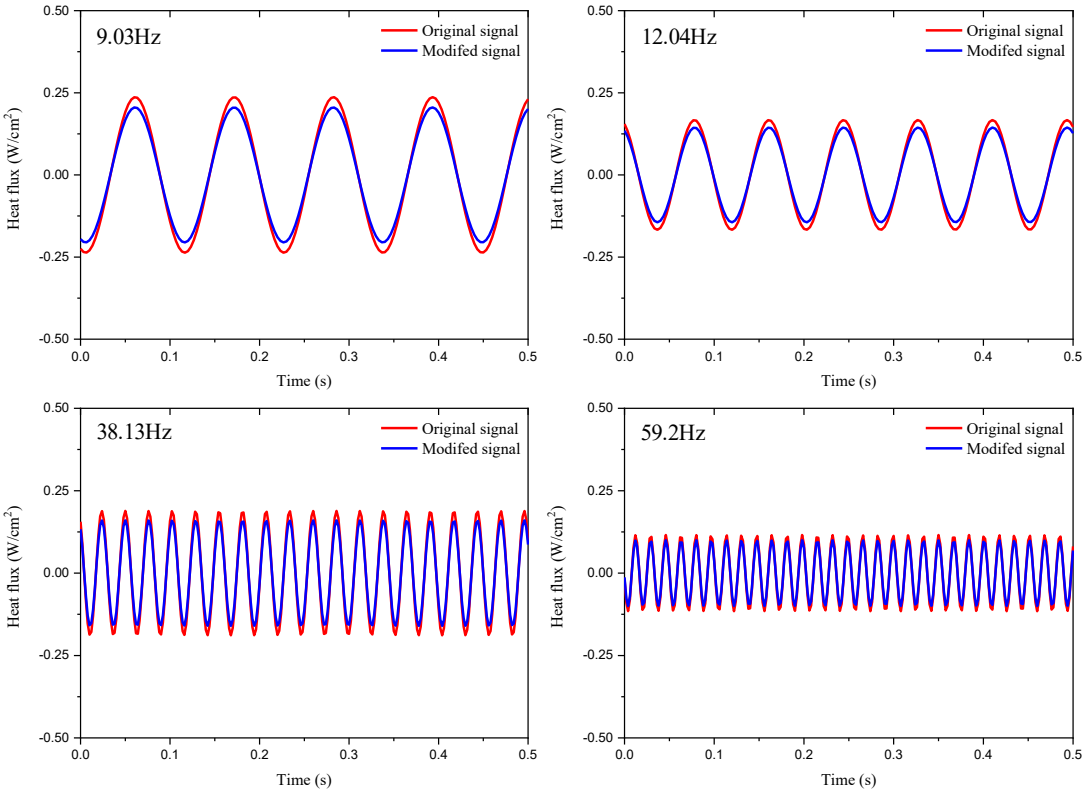

Fig. 14. Mono-frequency signals extracted from the heat flux signal

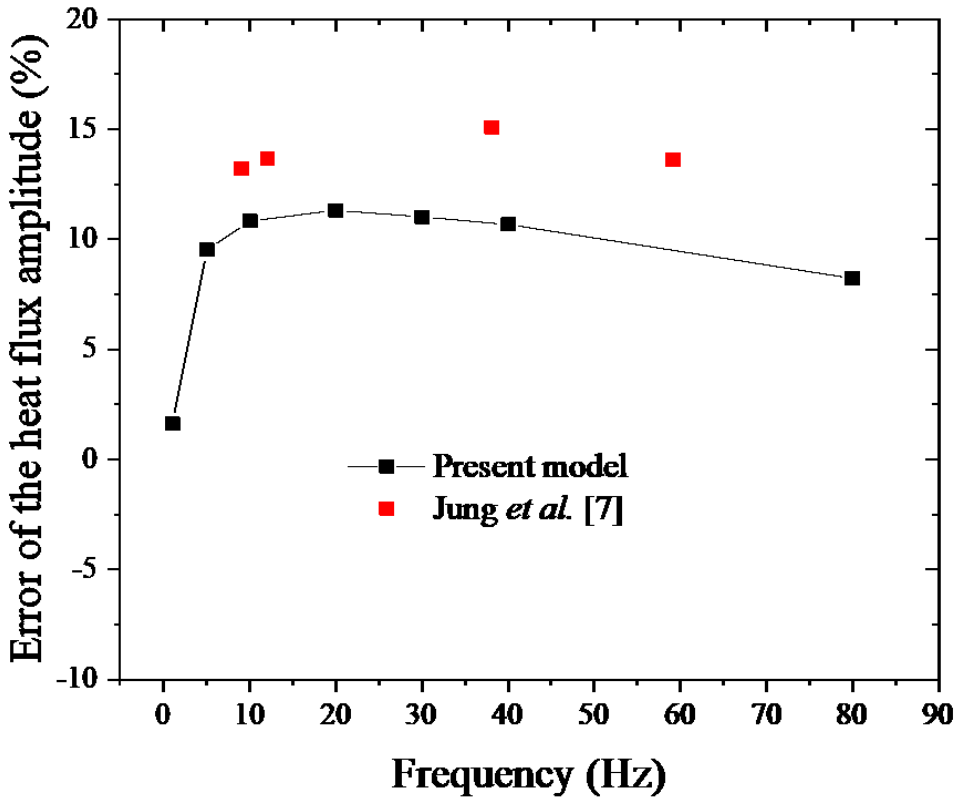

Fig. 15. Comparison of errors in the amplitude of heat flux

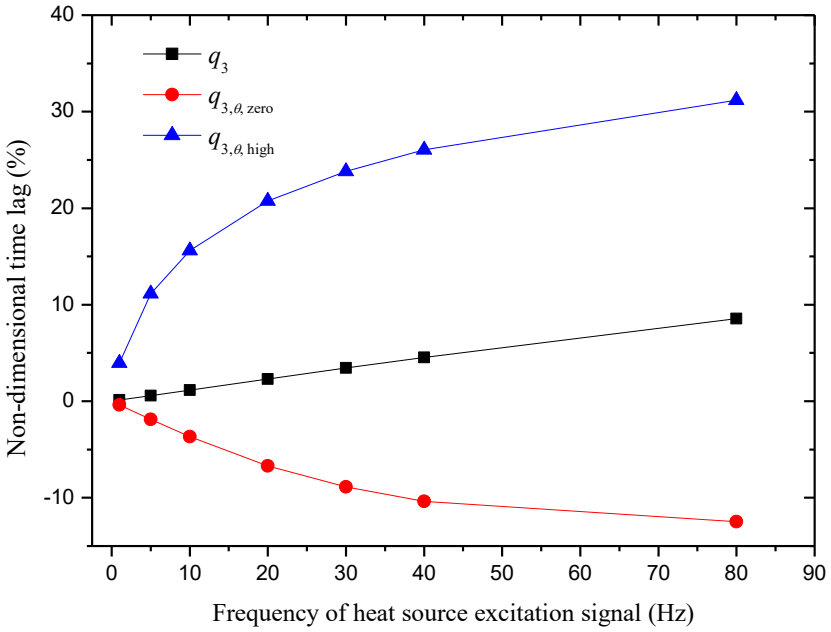

Fig. 16. Non-dimensional time lag of heat flux signals (q_3, $q_{3,\theta,\text{zero}}$, $q_{3,\theta,\text{high}}$)

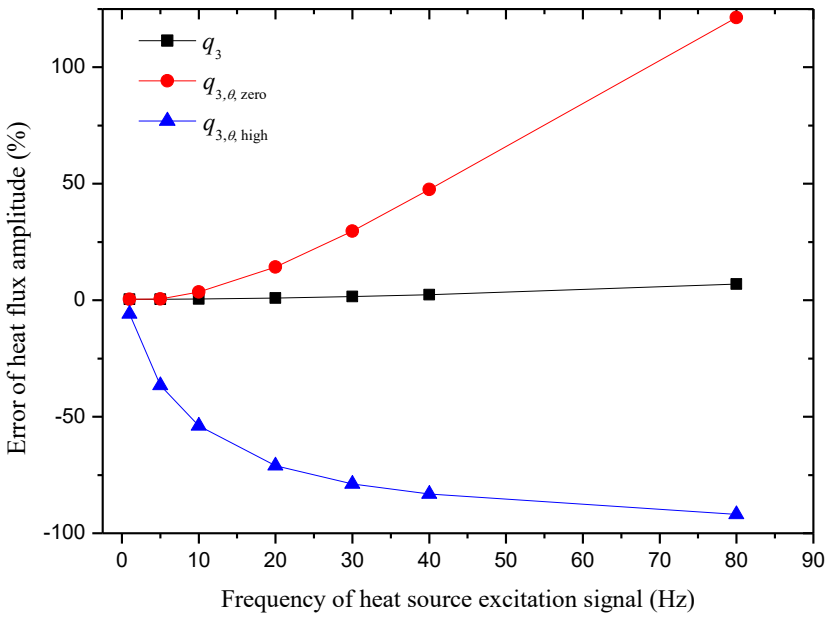

Fig. 17. Errors in the amplitude of heat flux signals (q_3, $q_{3,\theta,\text{zero}}$, $q_{3,\theta,\text{high}}$)

List of table captions

Table 1. Thermal properties of each layer in Fig. 5

Material	Density (kg/m^3)	Thermal conductivity (W/m-K)	Specific heat (J/kg-K)	Thickness (μm)
Nichrome	8400	11.3	450	0.5
SiO_2	2196	1.2	1000	0.5
ITO	7140	11	753	0.5
Polyimide	1420	0.12	1100	10
Silicon	2320	148	700	500

Table 2. Boundary conditions for numerical simulation to obtain q_3, $q_{3,\mathrm{IR}}$ and $q_{3,\mathrm{IR,th}}$

		T, q	T_{IR}, q_{IR}	$T_{\mathrm{IR,th}}$, $q_{\mathrm{IR,th}}$
Number of layers		5	2	2
Boundary conditions	Thermal contact resistance ($\mathrm{cm^2K/W}$)	$\theta_{1,2}$=10 $\theta_{2,3}$=10 $\theta_{3,4}$=0.1 $\theta_{4,5}$=0.1	$\theta_{4,5}$=0	$\theta_{4,5}$=0.1
	Top surface	h_{t}=9.4 $\mathrm{W/(m^2K)}$	$T(x_3,t)$	$T(x_3,t)$
	Bottom surface	h_{b}=4.7 $\mathrm{W/(m^2K)}$	h_{b}=4.7 $\mathrm{W/(m^2K)}$	h_{b}=4.7 $\mathrm{W/(m^2K)}$

Table 3. Boundary conditions for numerical simulation to obtain $q_{3,\theta,\text{zero}}$, $q_{3,\theta,\text{high}}$

		$T_{\theta,\text{zero}}$, $q_{\theta,\text{zero}}$	$T_{\theta,\text{high}}$, $q_{\theta,\text{high}}$
Number of layers		5	5
Boundary conditions	Thermal contact resistance (cm^2K/W)	$\theta_{1,2}=0$ $\theta_{2,3}=0$ $\theta_{3,4}=0$ $\theta_{4,5}=0$	$\theta_{1,2}=30$ $\theta_{2,3}=30$ $\theta_{3,4}=30$ $\theta_{4,5}=30$
	Top surface	h_t=9.4 W/(m^2K)	h_t=9.4 W/(m^2K)
	Bottom surface	h_b=4.7 W/(m^2K)	h_b=4.7 W/(m^2K)